PCCP

Accepted Manuscript

ROYAL SOCIETY OF CHEMISTRY

www.rsc.org/pccp

Journal Name

ARTICLE

Structure of Chloromethyl Thiocyanate, CH_2ClSCN, in Gas and Crystalline Phases

Received 00th January 20xx,
Accepted 00th January 20xx

DOI: 10.1039/x0xx00000x

www.rsc.org/

Y. Berrueta Martínez,[a] L. S. Rodríguez Pirani,[a] M. F. Erben,[a] C. G. Reuter,[b] Y. V. Vishnevskiy,[b] H. G. Stammler,[b] N. W. Mitzel,[b] and C. O. Della Védova[a]

The structural and conformational properties of chloromethyl thiocyanate, CH_2ClSCN, were studied in the solid and in the gas phase using *in situ* low-temperature single-crystal X-ray diffraction experiments (XRD) and gas electron diffraction (GED), respectively. Depending on the mutual orientation of the Cl–C bond and the -SCN group, two conformations, *gauche* and *anti,* were found to coexist in the gas phase. The *gauche* conformer, with a dihedral angle δ(ClC-SC) = 71.8(4)º, is the most stable form, with an abundance of 89(3)% at ambient temperature. High level quantum-chemical calculations at the CCSD(T)/cc-pVTZ level of approximation reproduce these experimental results. In the solid state only *gauche* conformers were found to be present. The crystal structure shows specific intermolecular interactions including chalcogen-type interactions. The experimental electron density distribution was determined by high-angle X-ray diffraction. The Atoms in Molecules (AIM) Theory was applied to analyze the charge density topology a for a better characterization of intermolecular interactions present in the crystal.

1. Introduction

Isothiocyanate species (R−N=C=S) are, in general, energetically favored over their thiocyanate (R–S–C≡N) bond isomers. Therefore, the thiocyanate isomers are rather elusive and often difficult to isolate. This fact has recently been evidenced in the synthesis of intervenolin, during which an intermediate thiocyanate species spontaneously undergoes a pivotal rearrangement to the corresponding isothiocyanate isomer.[1] The isomerization mechanisms have been studied with detail, as in the case for benzyl and alkyl (especially *tert*-butyl) thiocyanates, which rearrange via an ion pair mechanism in solution.[2,3,4,5,6,7] Recently we were successful in determining the isomerization process and fundamental properties −including the conformation and molecular structures− of acyl−thio and acyl−isothio cyanates, such as XC(O)SCN/XC(O)NCS, with X = F, [8] Cl[9] and OCH_3.[10]

Previous studies on the conformation and molecular structure of simple thiocyanate mainly by using microwave are available in the literature. For instance, the microwave spectrum of CH_3SCN was early reported as a foundational application of microwave absorption spectroscopy in determining the structure of asymmetric molecules.[11] The microwave spectrum of ethyl thiocyanate, CH_3CH_2SCN, was also investigated by Bjørseth and Marstokk resulting in the presence of only one conformer having the CH_3 group and C≡N group *gauche* to one another, the total dipole moment being 4.01±0.12 D.[12] A second, less stable trans conformer was also reported in the liquid phase by Durig *et al.* and an enthalpy difference of 1.68±0.07 kcal mol^{-1} between the *gauche* and *trans* conformers was determined from a variable-temperature Raman study.[13] More recent experiments were conducted by Møllendal and Guillemin for a series of thiocyanates, including CH_2=C=CHSCN (propa-1,2-dienly thiocyanate)[14] and HC≡CCH_2SCN (propargyl thiocyanate).[15]

In an effort for an improved understanding of the molecular structure, including the determination of geometrical parameters, of thiocyanate species in both, the vapor and condensed phases, a series of simple halomethyl−thiocyanate species has been studied. In this article, results on chloromethyl thiocyanate, CH_2ClSCN, are presented.

Chloromethyl thiocyanate, CH_2ClSCN, shows excellent antifungal, nematicidal and bactericide activities. It is also used as an intermediate in the synthesis of 2−(thiocyanomethylthio)−benzothiazole, a widely used fungicide in the industrial manufacturing of leather.[16] Fundamental properties of CH_2ClSCN are scarcely available; they include an early vibrational study reported by Crowder[17,18] and a more recent report on its electronic structure.[19]

The analysis of both, single crystal X−ray diffraction (XRD) and gas electron diffraction (GED) patterns, offers structural and conformational information. In particular, XRD allows analyzing intermolecular interactions occurring in these

[a] *CEQUINOR (UNLP-CONICET), Departamento de Química, Facultad de Ciencias Exactas, Universidad Nacional de La Plata, 47 esq. 115, 1900 La Plata, República Argentina.*
[b] *Lehrstuhl für Anorganische Chemie und Strukturchemie, Universität Bielefeld, Universitätsstraße 25, 33615 Bielefeld, Germany.*

Electronic Supplementary Information (ESI) available: [details of any supplementary information available should be included here]. See DOI: 10.1039/x0xx00000x

systems, including chalcogen and hydrogen bonds, and their influence on the molecular structure. The study of the conformational equilibrium and structural parameters in crystal and gas phases and the investigation of intermolecular interactions in the solid state are the main focus of the present work. The involved chalcogen Cl···S–C and N···S–C interactions are relevant topics at the present. Such interactions have been studied in some detail, especially for bi-molecular complexes.[20] Intermolecular interactions of nitrogen functions with other atoms in A···N type bonds (A = Cl, S, P) have been compared by Scheiner *et al.* They have shown that these particular intermolecular types of bonding depend on electrostatic and inductive contributions.[20] Intermolecular chalcogen interactions in the crystal phase of the mentioned compounds are widely discussed in this work, especially in terms of their structure and energetic characteristics.

2. Experimental Section

Synthesis

A sample of CH_2ClSCN was prepared by reaction of CH_2ClSCl with KCN in diethyl ether and was subsequently purified by several trap-to-trap distillations.[21] The identity and purity of these compounds were verified using infrared spectroscopy.[17,18]

Instrumentation and Procedure

Quantum-chemical calculations. DFT[22] and MP2[23] calculations were performed using the Gaussian 03 suite of programs.[24] After the geometry optimization harmonic frequencies were calculated to prove the existence of a minimum on the potential hyper-surface. For support of the GED structural analysis analytical harmonic and numeric cubic force fields were calculated at the B3LYP/6-31G(d) and O3LYP/cc-pVTZ levels. These results were subsequently used to compute mean-square interatomic vibrational amplitudes and vibrational corrections to the equilibrium structure by the SHRINK program.[25,26,27] Coupled-cluster CCSD and CCSD(T)[28] analytical gradient-powered geometry optimizations were performed using the Cfour program package.[29] NBO[30] analyses were performed with the NBO 5.G program[31] incorporated in the Firefly suite of programs.[32]

Gas electron diffraction. The gas electron diffraction patterns were measured with the improved Balzers Eldigraph KD–G2 gas-phase electron diffractometer[33] at the University of Bielefeld. The experimental details are listed in Table S1.
Diffraction images were measured on the Fuji BAS-IP MP2 2025 imaging plates, which were scanned using the calibrated Fuji BAS-1800II scanner. The intensity curves (see Figures S1 – S2) were retrieved from the scanned diffraction images by applying the method described earlier.[34] Sector function and electron wavelength were as usually calibrated[35] using benzene diffraction patterns, recorded along with the substance under investigation. Experimental amplitudes were refined in groups (see Tables S1 – S2). For this purpose scale factors (one per group) were used as independent parameters. The ratios between different amplitudes in one group were fixed at the theoretical values.
Two sets of theoretical amplitudes and corrections, calculated from B3LYP/6-31G(d) and O3LYP/cc-pVTZ force fields, were tested in the refinements. Those calculated at the B3LYP/6-31G(d) level allowed to obtain better agreement with experimental data and were used in the final models. For CH_2ClSCN three GED models were used: (a) solely *anti* conformer, (b) solely *gauche* conformer and (c) a mixture of both conformers. The definitions for groups of refined amplitudes are given in Tables S1 and S2.

X-ray diffraction. High-angle crystallographic data of CH_2ClSCN were collected using a Nonius Kappa CCD diffractometer. A single crystal was grown *in situ* by slowly cooling the melt after establishing a solid–liquid equilibrium of the sample at 235.5 K in a sealed glass capillary. All but one very small seed crystal, which was selected optically via an additional microscope mounted at the diffractometer, was then melted by locally warming the sample and chilled very slowly with 1 K per hour to 231.5 K until one single crystal fills the whole frozen zone inside the capillary. Afterwards it was chilled to 160 K with 5 K/h and to 100 K with 60 K/h. At this temperature high redundant data were collected up to a 2θ value of 120°. Graphite-monochromated Mo Kα radiation was used (λ = 0.71073 Å) for data collection. The structure was solved and refined at first with SHELX–97, then a multipole refinement up to hexadecapoles was performed using the program package XD 2006[36] based on the Hansen and Coppens multipole formalism.[37] Details of the X-ray diffraction experiment are listed in Table 1.
CCDC 1020624 contains the supplementary crystallographic data for this paper. These data can be obtained free of charge from The Cambridge Crystallographic Data Centre via www.ccdc.cam.ac.uk/data_request/cif.

Table 1. Details of the X-ray diffraction experiment

Chemical formula	CH_2ClSCN
M_r	107.5
Unit cell, space group	monoclinic, $P2_1/n$
Temperature (K)	100(1)

a (Å)	4.0274(1)
b (Å)	11.5498(8)
c (Å)	9.3911(7)
β (°)	96.777(5)
V (Å^3)	433.78(5)
Z	4
ρ_{calc} (calculated) (g cm^{-3})	1.647
F(000)	216
Crystal color	Colorless
Crystal description	Cylindrical
Wavelength (Å)	0.71073
μ (mm^{-1})	1.16
Crystal size (mm)	0.3
Theta measurement range	3–60
Completeness to ϑ_{max}	99.5
Index range h, k, l	–9 / 9, –28 / 28, –22 / 22
Transm.$_{max/min}$	0.6587 / 0.4280
R before/after correct	0.1161 / 0.0454
Collected reflections	69952
Independent reflections	6721
R(int)	0.027
Data/restraints/parameters	4881 / 0 / 191
Goodness of fit in F^2	2.133
$R1$ / w$R2$ [observed refl.]	0.0191 / 0.0139
Observed refl. with	$I > 3\sigma(I)$
$R1$ / w$R2$ (complete data)	0.0311 / 0.0259
Extinction coefficient	0.0101(4)
$\rho_{max/min}$ (e Å^{-3})	0.04/–0.04
CCDC no.	1021027

3. Results and discussion

The molecular structure of CH_2ClSCN was determined by gas electron diffraction, by single crystal X-ray diffraction and by computational methods. In the first of the following sections we will first discuss the quantum-chemical results with focus on the conformational behavior, followed by a description and discussion of the molecular structure in the view of all methods applied, while the last section will attend to the intermolecular interactions in the solid state including a topological analysis of the electron density of CH_2ClSCN for which we succeeded in growing a crystal suitable for high-angle X-ray diffraction.

3.1 Computational chemistry

The molecular structure and conformational properties of CH_2ClSCN were quantum-chemically investigated by using two levels of approximations, B3LYP and MP2 in conjunction with the cc-pVTZ basis set. The calculated potential energy functions of internal rotation about the C1–S2 bond are shown in Figure 1. These curves predict that *gauche* is the most stable conformation for CH_2ClSCN, with ClC–SC dihedral angles around 70 and 80º. Maxima in the potential energy curves are observed for structures with eclipsed orientation between the halo-methyl and the SCN group (ClC–SC dihedral angle being 0º). Qualitative agreement is obtained between the two quantum-chemical methods used here. The B3LYP level, however, predicts lower energy barriers than the MP2 method.[38]

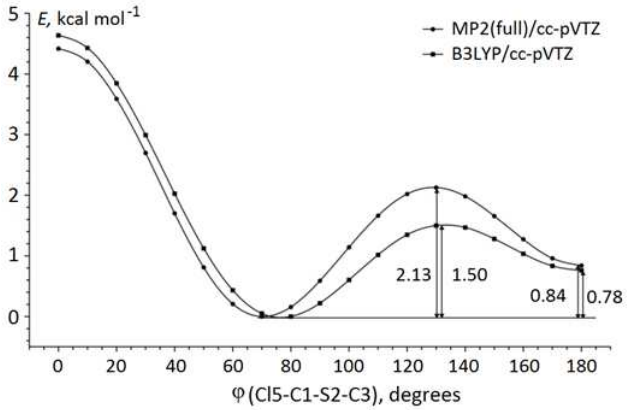

Figure 1. Potential energy functions of the internal rotation about the C1–S2 bond of CH_2ClSCN.

At the second stage of the theoretical analysis, the geometries of the two conformers were fully optimized including frequency calculations at the same levels of theory. The corresponding models for *gauche* and *anti* conformers of CH_2ClSCN are depicted in Figure 2. The predicted relative energies (ΔE) and Gibbs free energies (ΔG^0) are collected in Table 2. Using the Boltzmann distribution, the conformational compositions at 336 K listed in Table 2 were obtained for CH_2ClSCN taking into account that the *gauche* conformers are doubly degenerate by symmetry considerations. The *anti* conformer of CH_2ClSCN with a φ(Cl5–C1–S2–C3) = 180^0 belong to the C_S point group of symmetry and at the temperature of the GED experiment its abundance was predicted to be in the region between 15 and 18 %.

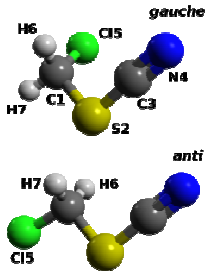

Figure 2. Molecular structure and atom numbering scheme of the *gauche* and *anti* conformers of CH_2ClSCN.

Table 2. Relative total Δ*E* and free Gibbs Δ*G* energies (kcal mol^{-1}) and abundances χ (%) of *anti* conformer of CH_2ClSCN

	CH_2ClSCN		
	ΔE^a	ΔG^a	X^a
B3LYP/cc-pVTZ	0.78	0.56	17.7
MP2(full)/cc-pVTZ	0.84	0.71	14.8

[a] Energies are relative to those of *gauche* conformers. Gibbs free energies were calculated using standard "uncoupled harmonic rotator – rigid oscillator" approximation. The abundances were calculated from free Gibbs energies for 336 K (CH_2ClSCN).

3.2 Molecular structures

Relevant geometric parameters obtained for the vapor (GED) and crystalline (XRD) phases of CH_2ClSCN, as well as that obtained by using theoretical calculations (CCSD(T)/cc-pVTZ) are compared in Table 3.

Table 3. Experimental and theoretical structural parameters of CH_2ClSCN[a]

	gauche				*anti*		
	GED		XRD	CCSD(T)	GED		CCSD(T)
	r_e	r_g	r_e	r_e	r_e	r_g	r_e
C1–S2	1.805(2)[1]	1.818(2)	1.8074(2)	1.814	1.821(2)[1]	1.835(2)	1.830
S2–C3	1.691(4)[2]	1.698(4)	1.6891(3)	1.699	1.692(4)[2]	1.698(4)	1.700
C3–N4	1.159(3)[3]	1.163(3)	1.1601(4)	1.164	1.159(3)[3]	1.164(3)	1.164
C1–Cl5	1.766(2)[4]	1.777(2)	1.7721(3)	1.775	1.762(2)[1]	1.773(2)	1.771
C1–H6	1.081[b]		1.10(2)	1.081	1.081[b]		1.081
C1–H7	1.083[b]		1.11(3)	1.083	1.081[b]		1.081
C1–S2–C3	99.8(15)[4]		98.00(1)	98.2	96.5(35)[6]		96.3
S2–C3–N4	178.2[b]		178.30(3)	178.2	179.6[b]		179.6
S2–C1–Cl5	113.5(3)[5]		113.35(2)	114.3	91.4(19)[9]		107.4
S2–C1–H6	108.5(13)[6]		109.8(4)	109.6	108.7(13)[6]		109.8
S2–C1–H7	104.1(13)[6]		104.6(4)	105.2	108.7(13)[6]		109.8
Cl5–C1–H6	107.4(13)[6]		108.2(4)	108.5	107.9(13)[6]		109.0
Cl5–C1–H7	107.5(13)[6]		108.6(4)	108.6	107.9(13)[6]		109.0
H6–C1–H7	116.1(54)[6]		112.5(6)	110.6	126.6(41)[6]		111.7
Cl5–C1–S2–C3	71.8(39)[7]	63.7(3)	62.16(2)	71.9	180.0[b]		180.0
x_i[d] %	89(3)		100	85	11(3)		15

[a] The parameters are given in Å and deg. Standard deviations are in parentheses and represent 3σ for GED and 1σ for XRD. Superscript numbers 1, 2, …, 9 indicate groups, in which parameters were refined with fixed differences. The CCSD(T) calculation was performed with cc-pVTZ basis set.

[b] Fixed parameter, see text for details.

[c] Dependent parameter.

[d] Conformational composition. Theoretical values were calculated for 336 K using the Boltzmann distribution and total energies.

3.2.1 Molecular structure in the gas phase. As mentioned above, a variety of theoretical models (100% *gauche*, 100% *anti* and a mixture of both conformers) were proposed in the refining steps for CH_2ClSCN. The agreement of radial distribution functions in each case as well as corresponding structural *R*-factors are given in Figure 4. Analysis of the experimental GED data reveals that for CH_2ClSCN the *gauche* conformer is the most stable one in the gas phase. Molecules with *anti* conformation were also detected in the gas phase at the temperature of the experiments (detailed in Table S1). For CH_2ClSCN the determination of the second conformer from GED data is straightforward due to a characteristic peak in the radial distribution function at r = 5.1 Å (see Figure 4). This signal can be attributed to the N4–Cl5 contribution in the *anti* conformer of CH_2ClSCN without any hesitation. As a result, the abundance of *anti* conformer in the gas phase was determined to be 11(3) % (3σ error indicated in parentheses).

Experimental results are generally in agreement with the theoretical values (Table 3) assuming the limited predicting power of the approximations used.

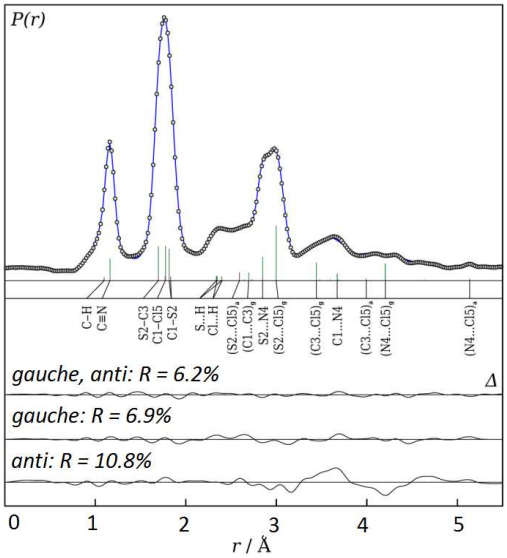

Figure 4. Experimental (circles) and model (line) radial distribution functions of CH_2ClSCN. The difference curves for tested models are given at the bottom. Subscript letters a and g indicate contributions related only to *anti* and *gauche* conformers.

A closer analysis of the conformation-structure relationships reveals that for CH_2ClSCN, C≡N bond lengths in gas phase are not perceptible to the change in conformation. The situation with the weaker C1–S2 bonds is more interesting. This bond length is correlated with the orientation of the C–Cl bond in the molecule connected to the SCN moiety. The shortest C1–S2 bond was observed for the more abundant *gauche* conformer of the CH_2ClSCN (r_g = 1.818(2) Å). The C1–S2 bond is

elongated when the C–Cl bond is *anti* oriented with respect to the S2–C3 bond.

It is well-known that the conformational properties affect the geometrical parameters mainly through hyperconjugative electronic effects, which strongly depend on the orientation of the interacting groups. We used NBO analyses in the B3LYP/cc-pVTZ approximation to study the dependence of the C1–S2 bond lengths on the conformation. The second order perturbation analysis within NBO scheme shows an interaction between one electron lone pair at the chlorine atom with the C1–S2 anti-bonding orbital, n(Cl)→σ*(C1–S2). The corresponding stabilization energies *E*(2) are 8.0 and 6.3 kcal mol^{-1} for the *gauche* and *anti* conformations, respectively. This type of interaction also leads to increased occupation numbers of the corresponding σ*(C1–S2) orbitals. In case of the *gauche* conformation the occupation number is slightly larger (0.05 *e*) than in the *anti* conformation (0.04 *e*). However, this fact does not explain the shortening of the C1–S2 bond in the *gauche* conformation. The described increased population of the σ*(C1–S2) orbital in the *gauche* conformation should lead to the weakening of the C1–S2 bond and, as a consequence, to its elongation. This contradicts to the experimentally observed values of bond lengths. On the other hand, the repulsion of lone pairs on the chlorine and sulfur atoms could be used to describe the founded geometrical relationships.

Figure 5 shows the comparison of relative positions of different combinations of lone pairs of electrons at the Cl and S atoms in CH_2ClSCN. Clearly, the *anti* form has the most

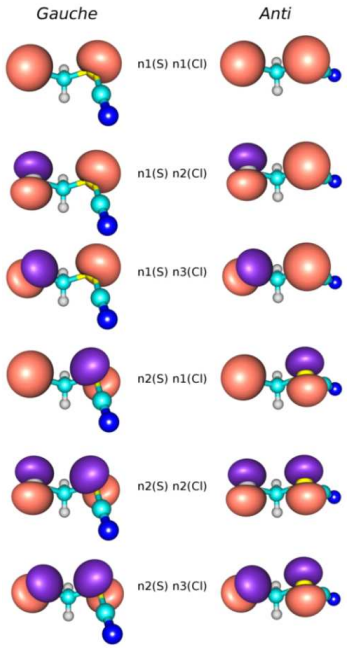

Figure 5. Comparison of positions of different combinations of electron lone pairs on the S and Cl atoms in CH_2ClSCN.

repulsive relative orientations of the lone pairs in case of n1(S)↔n1(Cl) and n2(S)↔n2(Cl). Consequently, the C1–S2 bond length increases to compensate for the repulsion. This simple model also explains the preference of the *gauche* over the *anti* conformation.

3.2.2 Molecular structure in solid state. Compound CH_2ClSCN crystallizes in the monoclinic system, space group $P2_1/n$. Its structure was determined by high-angle X-ray diffraction up to 2ϑ of 120° at low temperatures. We used the Hansen-Coppens formalism to extract the electron density distribution for this solid. This allows analyzing the electron density topology in terms of the Quantum Theory of Atoms in Molecules.[39] Electron density topology parameters are listed in Table 4, and the atomic charges calculated by integration of charge over the atomic basins are listed in Table 5.

In the crystal phase CH_2ClSCN adopts a *gauche* type conformation, with a dihedral angle δ(ClC–SC) equal to 62.2(2)° (Figure 6). Bond lengths refined to their expected values of 1.10(2) Å and 1.11(3) Å for C–H distances, 1.8074(2) Å for CH_2Cl–S and 1.6891(3) Å for S–CN distances, 1.1601(4) Å for C–N and 1.7721(3) Å for Cl–C distance.

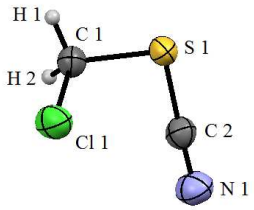

Figure 6. Molecular structure of CH_2ClSCN in the crystal as determined by X-ray diffraction at 100 K.

The electron densities at the bond critical points (bcp) reflect the nature of the chemical bonds with typical values for Cl–C and C–H covalent single bonds.[40] The C–S bonds show slightly different values at their bcps, with the CH_2Cl–S bond having a smaller value at 1.28(1) e Å–3 than the S–CN bond at 1.42(1) e Å–3. This reflects the small partial multiple bond character expressed in the Lewis formula $ClH_2C–S^{\oplus}=C=N^{\ominus}$ and is supported by the more positive corresponding Laplacian value ($-\nabla 2\rho$(bcp)) of 5.47(1) e Å–5 (compared to 4.62(1) e Å–5 for the other C–S bond). Expectedly, the highest electron density at the bcp is found for the N≡C triple bond at 3.43(1) e Å–3, with a corresponding very large value of the Laplacian at 38.1(1) e Å–5 compared with HCCH: ρ(bcp) = 2.93 e Å–3, $-\nabla 2\rho$(bcp) = 35.3 e Å–5 and N2: ρ(bcp) = 4.8 e Å–5.[41] The Laplacian values at the remaining bcp's also reveal the covalent nature of all these bonds. The electron density (a) and

the Laplacians (b) in the plane of the atoms C–S–C–N are shown in Figure 7.

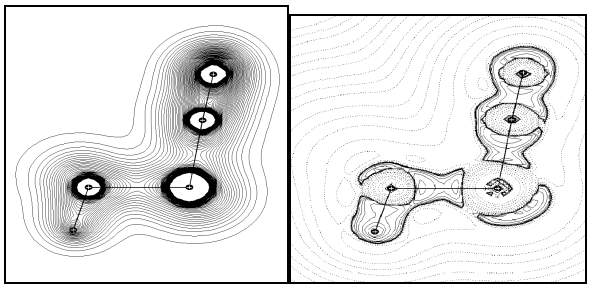

(a) **(b)**

Figure 7. Plot of electron density (a) and Laplacians (b) in the C-SCN plane.

Table 4. Electron density topology parameters for selected bonds in CH_2ClSCN as determined by high–angle X–ray diffraction. Electron densities ρ(bcp) are given in e Å^{-3}, Laplacians $-\nabla^2\rho$(bcp) in e Å^{-5}, distances in Å. Also given are the curvature components λ and the ellipiticity ε.

bond i–j	ρ(bcp)	$-\nabla^2\rho$ (bcp)	r_{ij}	r_{bcp-i}	r_{bcp-j}	λ_1	λ_2	λ_3	ε
Cl(1)–C(1)	1.28(1)	2.40(3)	1.773	0.978	0.794	−7.62	−7.17	12.39	0.06
S(1)–C(1)	1.24(1)	4.62(3)	1.808	0.938	0.870	−7.46	−6.25	9.09	0.19
S(1)–C(2)	1.42(1)	5.47(4)	1.689	0.830	0.860	−8.54	−6.86	9.92	0.24
N(1)–C(2)	3.43(3)	38.1(2)	1.160	0.721	0.440	−29.11	−28.56	19.57	0.02
C(1)–H(1)	1.88(11)	23.2(4)	1.098	0.760	0.338	−19.10	−17.73	13.64	0.08
C(1)–H(2)	1.81(11)	22.1(4)	1.114	0.753	0.361	−17.76	−16.64	12.32	0.07

Letters i and j correspond to the label of the atoms.

The charges give an enlightening picture of bonding of CH_2ClSNC and the importance of the alternating charge principle in chemical bonding. The most negatively charged atom N is the neighbor of the most positive C. The sulfur atom, although surrounded by two about as electronegative carbon atoms is positively charged. This again gives some weight to the Lewis formula $ClH_2C–S\oplus=C=N\ominus$, although such formal charges should not necessarily be mixed up with physical charges. C(1) of the chloromethyl group bears a higher negative charge than the adjacent chlorine atom.

Table 5. AIM atomic charges of CH_2ClSCN as determined by high-angle X-ray diffraction

atom	q/e
Cl(1)	–0.13
S(1)	0.20
N(1)	–0.84
C(1)	–0.27
C(2)	0.56
H(1)	0.22
H(2)	0.26

3.2.3 Inter-molecular interactions in crystal phase. Analysis of the crystal packing topology manifested the non-bonding interactions of non–carbon atoms with distances shorter than the sum of the van der Waals radii of the involved atoms as listed in Table 6. The strongest shortening is observed for the N···H hydrogen bridge and the chalcogen bond directed opposite to the SCN ligand at an angle of 175.1(1)° near the 180° directionality expected for a typical chalcogen bond with a positive electrostatic potential orientated in the NC-S direction (σ-hole).[42] A chain running along the unit cell axis is formed by these two contacts as illustrated in Figure 8a. The chains are connected via non-classical Cl···H hydrogen bridges to planes perpendicular b (Figure 8b). These planes are connected by the weaker chalcogen interactions along b to a three dimensional framework (see Figure 8c). The C–Cl···Cl and the CH_2Cl–S···Cl units show distances of 3.50(1) Å and 3.46(1) Å and angles of 128.8(1)° and 172.2(1)°, respectively. The first angle is very far from the expected 180° directionality for a σ-hole interaction and both contacts show only a little shortening compared to the expected van der Waals distance. This suggests that they are not typical secondary bonds of the Cl···Cl resp. Cl···S halogen bond type. However, the Cl···S interaction fits into the geometry of a nucleophilic center, provided by the S atom.[43,44] As each sulfur atom is involved in two chalcogen-type interactions, the coordination around the sulfur atom is square planar (Figure 9). In 1970 Konnert and Britton[45] described this phenomenon for several thiocyanates, such as $(CH_2SCN)_2$, $S(CN)_2$, and $(CH_3)_2SC(CN)_2$. Except for two cases, $CH_2(SCN)_2$ and tetracyano-l,4-dithiine, the square-planar environment around the sulfur atom seems to be the general structure adopted by sulfur atoms in solid thiocyanates.

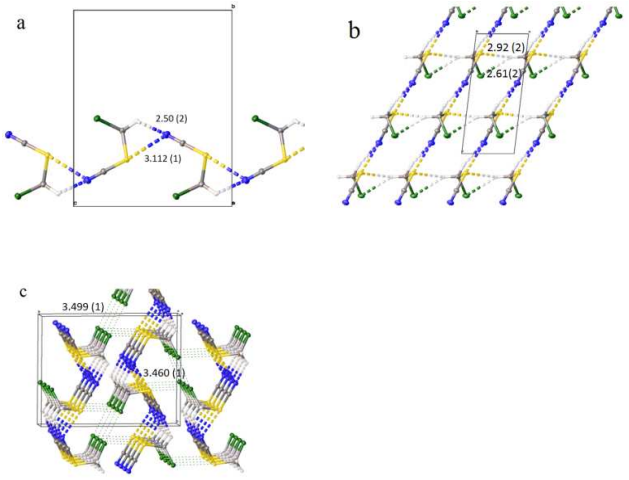

Figure 8. Crystal packing and non-bonding intermolecular interactions of CH_2ClSCN determined from X-ray diffraction at 100 K. a chain along c, b plane perpendicular b, c. 3D framework.

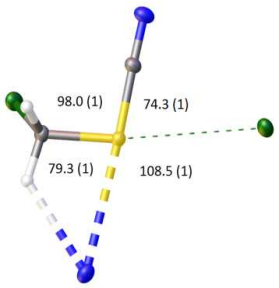

Figure 9. Angles in deg at square−planar coordinated sulfur atom in CH_2ClSCN.

Table 6. CH_2ClSCN non−bonding intermolecular interactions characteristics

Intermolecular contact	Distance (Å)	Angle (degrees)	Sum of van der Waals radii (Å)	Shortening (Å)	Contact type proposed
C-Cl···Cl' [1]	3.499(1)	128.8(1)	3.50	0.01	None
H_2ClCCl···S-C' [2]	3.460(1)	172.2(1)	3.55	0.04	Chalcogen bond
C-Cl···H' [3]	2.81(2)	75.2(4)	2.95	0.14	Hydrogen bond
NCS···N' [4]	3.112(1)	175.1(1)	3.35	0.23	Chalcogen bond
C-N···H' [4]	2.50(2)	163.7(3)	2.75	0.25	Hydrogen bond
NC-S···H' [3]	2.92(2)	119.5(2)	3.00	0.08	Hydrogen bond

As van der Waals radii were used: Cl 1.75 Å, S 1.80 Å, N 1.55 Å, H 1.2 Å. Symmetry codes for equivalent atoms marked with ': [1] 1–*x*, 1–*y*, 2–*z*; [2] 3/2–*x*, –½+*y*, 3/2–*z*; [3] 1+*x*, *y*, *z*; [4] *x*–½, –½–*y*, ½+*z*.

As a second we further selected to look at the experimental electron density determined from the high-angle X-ray diffraction data of CH_2ClSCN. A molecular graph, showing the molecule (intermolecular atomic interaction lines) and its topological connectivities to neighboring molecules in the crystal is shown in Figure 10, the intra- and intermolecular electron density topology parameters are listed in Table 7.

Table 7. Electron density topology parameters for selected intermolecular interactions in CH_2ClSCN as determined by high-angle X-ray diffraction. Electron densities ρ(bcp) are given in *e* Å^{-3}, Laplacians $-\nabla^2\rho$(bcp) in *e* Å^{-5}, distances in Å. Also given are the curvature components λ and the ellipticity ε.

bond i–j	ρ(bcp)	$-\nabla^2\rho$ (bcp)	r_{ij}	r_{bcp-i}	r_{bcp-j}	λ_1	λ_2	λ_3	ε
Cl···Cl' [1]	0.04(1)	−0.55(1)	3.499	1.750	1.749	−0.10	−0.10	0.75	0.01
Cl···S' [2]	0.05(1)	−0.55(1)	3.462	1.729	1.733	−0.11	−0.10	0.75	0.06
H···Cl' [3]	0.04(1)	−0.42(1)	2.821	1.057	1.764	−0.13	−0.10	0.66	0.34
S···N' [4]	0.07(1)	−0.80(1)	3.112	1.653	1.459	−0.18	−0.16	1.14	0.14
H···N' [4]	0.06(1)	−0.87(1)	2.532	1.053	1.479	−0.18	−0.12	1.18	0.50
H···S' [1]	0.04(1)	−0.38(1)	2.936	1.079	1.856	−0.12	−0.07	0.57	0.57

Symmetry codes for equivalent atoms marked with ' [1] 1–*x*, 1–*y*, 2–*z*; [2] 3/2–*x*, ½+*y*, 3/2–*z*; [3] *x*–1, *y*, *z*; [4] ½+*x*, ½–*y*, *z*–½

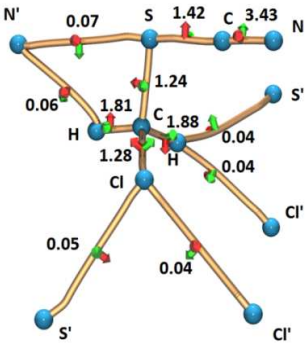

Figure 10. Intra- and intermolecular atomic interaction lines and electron densities at the bcp's of CH_2ClSCN in the solid state as determined by AIM topological analysis of an electron density distribution derived from high-angle X-ray diffraction data. The atoms labelled with ' belong to symmetry equivalent neighbor molecules, symmetry codes and esd's see Table 9.

The connections by atomic interaction lines (AIL) between different molecules reflect the picture obtained by looking at geometrical close contacts. Every close contact shows an AIL, the electron densities at the bcps correspond to the shortening of the van der Waals contacts by trend and also the contacts falling little below the expected value show an AIL despite the fact of the non-fitting C–Cl···Cl angle of 128.1(1)°, which is contradictory to the distance criterion. However, all AIL's are characterized by very low electron density and demonstrate the weakness of such interactions.

In order to confirm the nature of the intermolecular interactions, the second-order perturbation stabilization energies *E*(2) associated to the charge transfer between electron donor and acceptor orbitals corresponding to adjacent molecules were calculated at the NBO B3LYP/6-311+G(d) level of approximation.

The σ*(S–C) nature of the charge acceptor orbitals denotes the typical σ-hole[42] involved in the mentioned chalcogen

interactions. According to the calculations, the donor orbitals correspond to lone pair orbitals of nitrogen or chlorine atoms. These results are in agreement with the experimental angles described above. Moreover, there is a clear correlation between the calculated stabilization energy $E(2)$ (0.85 and 0.62 kcal mol^{-1} for N···S and Cl···S, respectively) and the corresponding shortening effect for each interaction (0.23 Å for N···S and 0.04 Å for Cl···S). Nevertheless, it is insufficient only to consider the charge transfer interactions in order to study chalcogen interactions. Other effects such as dispersion contributions, electrostatic effects and polarizations should also be taken into account.[42]

4. Conclusions

Crystals of CH_2ClSCN contain the most stable conformation of this molecule: *gauche*. Otherwise, the molecular structure in the solid state is generally in good agreement with that in gas phase, specially taking into account that we compare structural parameters different by nature: an rα-type structure from XRD with re parameters from GED.

The lengths of both C–S bonds are similar in the gas and crystal phases. The same holds for the angles with a few exceptions, which could be attributed to intermolecular interactions in the solid state. Interestingly, the C1–S2 bond length changes with a change of conformation in the gas phase. This fact was explained in terms of repulsive relative orientations between S and Cl lone pairs of electrons. The C1–S2 length is longer in the *anti* conformation than in the more stable *gauche* conformation due to this destabilizing interaction.

In the crystal structure several intermolecular interactions, in particular chalcogen interactions, have been detected and analyzed by means of structural parameters and theoretical calculations. The nature of charge transfer of these interactions is revealed in the performed NBO calculations where the typical sigma-hole (σ*(S–C)) was evidenced.

Acknowledgements

The authors thank Deutsche Forschungsgemeinschaft (DFG) for the scholarship of Y. B. M. in Germany and support of the core facility GED@BI, the Alexander von Humoldt Stiftung (stipend for Y. V. V.), Agencia Nacional de Promoción Científica y Técnica (CNPCYT), Consejo Nacional de Investigaciones Científicas y Técnicas (CONICET), Comisión de Investigaciones de la Provincia de Buenos Aires (CIC), Facultad de Ciencias Exactas, Universidad Nacional de La Plata (UNLP) and Bielefeld University for financial support.

Notes and references

1 H. Abe, M. Kawanda, H. Inoue, S. Ohba, A. Nomoto, T. Watanabe and M. Shibasaki, Org. Lett., 2013, 15, 2124.
2 A. Iliceto, A. Fava, U. Mazzucato, O. Rosseto, J. Am. Chem. Soc., 1961, 83, 2729.
3 A. Fava, A. Iliceto, A. Ceccon, P. Koch, J. Am. Chem. Soc., 1965, 87, 1045.
4 A. Fava, A. Iliceto, S. Bresadola, J. Am. Chem. Soc., 1965, 87, 4791.
5 R. Loos, S. Kobayashi, H. Mayr, J. Am. Chem. Soc., 2003, 125, 14126.
6 P. A. S. Smith, D. W. Emerson, J. Am. Chem. Soc., 1960, 82, 3076.
7 R. Koch, C. Wentrup, J. Org. Chem., 2013, 78, 1802–1810.
8 L. A. Ramos, S. E. Ulic, R. M. Romano, M. F. Erben, C. W. Lehmann, E. Bernhardt, H. Beckers, H. Willner, C. O. Della Védova, Inorg. Chem., 2010, 49, 11142-11157
9 L. A.Ramos, S. E. Ulic, R. M. Romano, M. F. Erben, Y. V. Vishnevskiy, C. G. Reuter, N. W. Mitzel, H. Beckers, H. Willner, X. Zeng, E. Bernhardt, M. F. Ge, S. Tong, C. O. Della Védova, J. Phys. Chem. A., 2013, 117, 2383-2399.
10 S. Torrico-Vallejos, M. F. Erben, M. F. Ge, H. Willner, C. O. Della Védova, J. Phys. Chem. A., 2010, 114, 3703-3712.
11 C. I. Beard, B. P. Dailey, J. Am. Chem. Soc., 1949, 71, 929-936.
12 A. Bjørseth, K. M. Marstokk, J. Mol. Struct., 1972, 11, 15–23.
13 J. R. Durig, J. F. Sullivan, H. L. Heusel, J. Phys. Chem., 1984, 88, 374–380.
14 G. C. Cole, H. Møllendal, J. C. Guillemin, J. Phys. Chem. A., 2007, 111, 2542-2546.
15 H. Møllendal, A. Konovalov, J. C. Guillemin, J. Phys. Chem. A., 2010, 114, 2300-2305.
16 L. Muthusubramanian, R. B. Mitra, S. Rajkumar, V. S. Sundara Rao, J. Chem. Tech., Biotech. 1998, 72, 164–168.
17 G. A. Crowder, J. Chem. Phys., 1967, 47, 3080–3081.
18 G. A. Crowder, Spectrosc. Lett., 1986, 19, 713–719.
19 L. S. Rodríguez Pirani, M. Geronés, C. O. Della Védova, R. M. Romano, A. Fantoni, R. Cavasso-Filho, C. Ma, M. Ge, M. F. Erben, J. Phys. Chem. A., 2012, 116, 231-241.
20 U. Adhikari, S. Scheiner, J. Phys. Chem A., 2012, 116, 3487–3497.
21 H. Brintzinger, K. Pfannstiel, H. Koddebusch, K. E. Kling, Chem. Ber., 1950, 83, 87–90.
22 Parr, R. G.; Yang, W. Oxford University Press, New York, USA, 1989.
23 C. Møller, M. S. Plesset, Phys. Rev., 1934, 46, 618–622.
24 Gaussian 03, Revision C.02, Frisch, M. J.; Trucks, G. W.; Schlegel, H. B.; Scuseria, G. E.; Robb, M. A.; Cheeseman, J. R.; Montgomery, Jr., J. A.; Vreven, T.; Kudin, K. N.; Burant, J. C.; Millam, J. M.; Iyengar, S. S.; Tomasi, J.; Barone, V.; Mennucci, B.; Cossi, M.; Scalmani, G.; Rega, N.; Petersson, G. A.; Nakatsuji, H.; Hada, M.; Ehara, M.; Toyota, K.; Fukuda, R.; Hasegawa, J.; Ishida, M.; Nakajima, T.; Honda, Y.; Kitao, O.; Nakai, H.; Klene, M.; Li, X.; Knox, J. E.; Hratchian, H. P.; Cross, J. B.; Bakken, V.; Adamo, C.; Jaramillo, J.; Gomperts, R.; Stratmann, R. E.; Yazyev, O.; Austin, A. J.; Cammi, R.; Pomelli, C.; Ochterski, J. W.; Ayala, P. Y.; Morokuma, K.; Voth, G. A.; Salvador, P.; Dannenberg, J. J.; Zakrzewski, V. G.; Dapprich, S.; Daniels, A. D.; Strain, M. C.; Farkas, O.; Malick, D. K.; Rabuck, A. D.; Raghavachari, K.; Foresman, J. B.; Ortiz, J. V.; Cui, Q.; Baboul, A. G.; Clifford, S.; Cioslowski, J.; Stefanov, B. B.; Liu, G.; Liashenko, A.; Piskorz, P.; Komaromi, I.; Martin, R. L.; Fox, D. J.; Keith, T.; Al-Laham, M. A.; Peng, C. Y.; Nanayakkara, A.; Challacombe, M.; Gill, P. M. W.; Johnson, B.; Chen, W.; Wong, M. W.; Gonzalez, C.; and Pople, J. A.; Gaussian, Inc., Wallingford CT, 2004.
25 V. A. Sipachev, J. Mol. Struct., 2004, 693, 235–240.
26 V. A. Sipachev, J. Mol. Struct., 2001, 567–568, 67–72.
27 V. A. Sipachev, Struct. Chem., 2000, 11, 167–172.
28 K. Raghavachari, G. W. Trucks, J. A. Pople, Chem. Phys. Lett., 1989, 157, 479–483.
29 M. E. Harding, T. Metzroth, J. Gauss, A. J. Auer, Chem. Theory Comput., 2008, 4, 64–74.

30 J. P Foster, F. Weinhold, J. Am. Chem. Soc., 1980, 102, 7211–7218.
31 E. D. Glendening, J. K. Badenhoop, A. E. Reed, J. E. Carpenter, J. A. Bohmann, C. M. Morales, F. Weinhold, NBO 5.G program, Theoretical Chemistry Institute, University of Wisconsin, 2001.
32 A. A. Granovsky, Firefly version 7.1.G, http://classic.chem.msu.su/gran/firefly/index.html.
33 R. J. F. Berger, M. Hoffmann, S. A. Hayes, N. W. Mitzel, Z. Naturforsch., 2009, 64b, 1259–1268.
34 Yu. V. Vishnevskiy, J. Mol. Struct., 2007, 833, 30–41.
35 Yu. V. Vishnevskiy, J. Mol. Struct., 2007, 871, 24–32.
36 A. Volkov, P. Macchi, L. J. Farrugia, C. Gatti, P. R. Mallinson, T. Richter, T. Koritsanszky, 2006, XD2006SHELXTL 6.10, Bruker-AXS X-Ray Instrumentation Inc., Madison, WI, 2000.
37 N. K. Hansen, P. Coppens, Acta Cryst., 1978, A34, 909–921SHELXTL 6.10, Bruker-AXS X-Ray Instrumentation Inc., Madison, WI, 2000.
38 B. J. Lynch, D. G. Truhlar, J. Phys. Chem. A., 2001, 105, 2936–2941
39 a) R. F. W. Bader, Atoms in Molecules: A Quantum Theory, Clarendon Press, Oxford, 1990; b) P. L. A. Popelier, Atoms in Molecules – An Introduction, Prentice Hall, 2000.
40 C. F. Matta, R. J. Boyd, The Quantum Theory of Atoms in Molecules, Wiley–VCH, Weinheim, 2007.
41 D. W. H. Rankin, N. W. Mitzel, C. A. Morrison, Structural Methods in Molecular Inorganic Chemistry (Inorganic Chemistry: A Textbook Series) 1st edition, John Wiley & Sons, Chichester, February 2013.
42 a) R. G. Gonnade, M. S. Shashidhar, M. M. J. Bhadbhade, Ind. Institute Sci., 2007, 87, 149–165; b) P. Politzer, J. S. Murray, ChemPhysChem., 2013, 14, 278; c) J. S. Murray, P. Politzer, T. Clark, Phys. Chem. Chem. Phys., 2013, 15, 11178.
43 D. Manna, G. Mugesh, J. Am. Chem. Soc., 2012, 134, 4269–4279.
44 W. Wang, B. Ji, Y. Zhang, J. Phys. Chem. A., 2009, 113, 8132–8135.
45 J. H. Konnert, D. Britton, Acta Crystallogr. Sect. B., 1971, 27, 781–786.